Electronic Supplementary Material (ESI) for Nanoscale.
This journal is @The Royal Society of Chemistry 2019

Supplementary Material

Thermally driven homonuclear-stacking phase of MoS_2 through desulfurization

Young Hun Hwang,[#,a,c] Won Seok Yun,[#,b] Gi-Beom Cha,[a] Soon Cheol Hong,*[,a] and Sang Wook Han*[,a]

[a]Department of Physics and Energy Harvest-Storage Research Center (EHSRC), University of Ulsan, Ulsan 44610, Republic of Korea.

[b]Department of Emerging Materials Science, DGIST, Daegu 42988, Republic of Korea.

[c]Present address: Electricity & Electronics and Semiconductor Applications, Ulsan College, Ulsan 44610, Republic of Korea

[#]These authors contributed equally to this work.

[*]Corresponding e-mail: schong@ulsan.ac.kr (S.C.H.); swhan72@ulsan.ac.kr (S.W.H.).

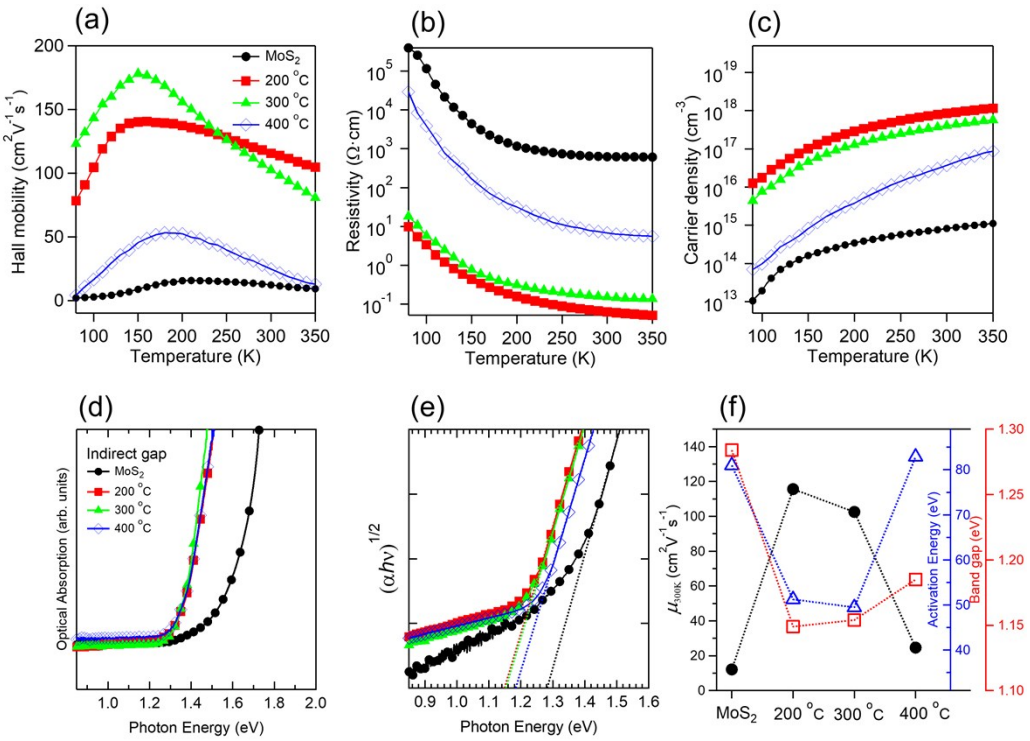

Fig. S1 The influence of N_2 annealing on the transport and optical of the single-crystalline MoS_2. (a–c) Temperature dependence of Hall mobility, Hall resistivity and carrier concentration. (d) Optical absorption coefficient shows the dependence of $(\alpha h\nu)^{1/2}$ on the photon energy ($h\nu$). (e) Extrapolating the linear part of each curve toward the energy axis gives the corresponding indirect bandgap energy (E_g). (f) Hall mobility at 300 K (left), activation energy and optical bandgap (right).

Single-crystalline bulk MoS_2 samples were annealed within a furnace filled with nitrogen gas as a function of temperature. Resistivity was measured using the Van der Pauw method, and carrier density and Hall mobility were determined from the Hall coefficient measured using a Hall measurement system (HMS 5000, ECOPIA21). Hall mobility (μ) is derived as a function of $\mu = \frac{\sigma}{ne}$, where n is the carrier density and e is the electron charge. The optical bandgap energy was determined from UV-VIS-NIR absorption spectra. Analysis was carried out using a Carry 5000 UV/Vis/NIR spectrometer (Varian). The bandgap energy of the optical absorption was derived using the relation $\alpha = A/h\nu(E - E_g)^n$ where A is a constant, $h\nu$ is the incident photon energy, and the exponent n depends on the kind of optical transition. Activation energy is derived from the temperature dependence of conductivity

using the equation $\sigma = \sigma_0 e^{-E_a/k_B T}$, where σ_0 is a pre-exponential factor, E_a is the activation energy, k_B is

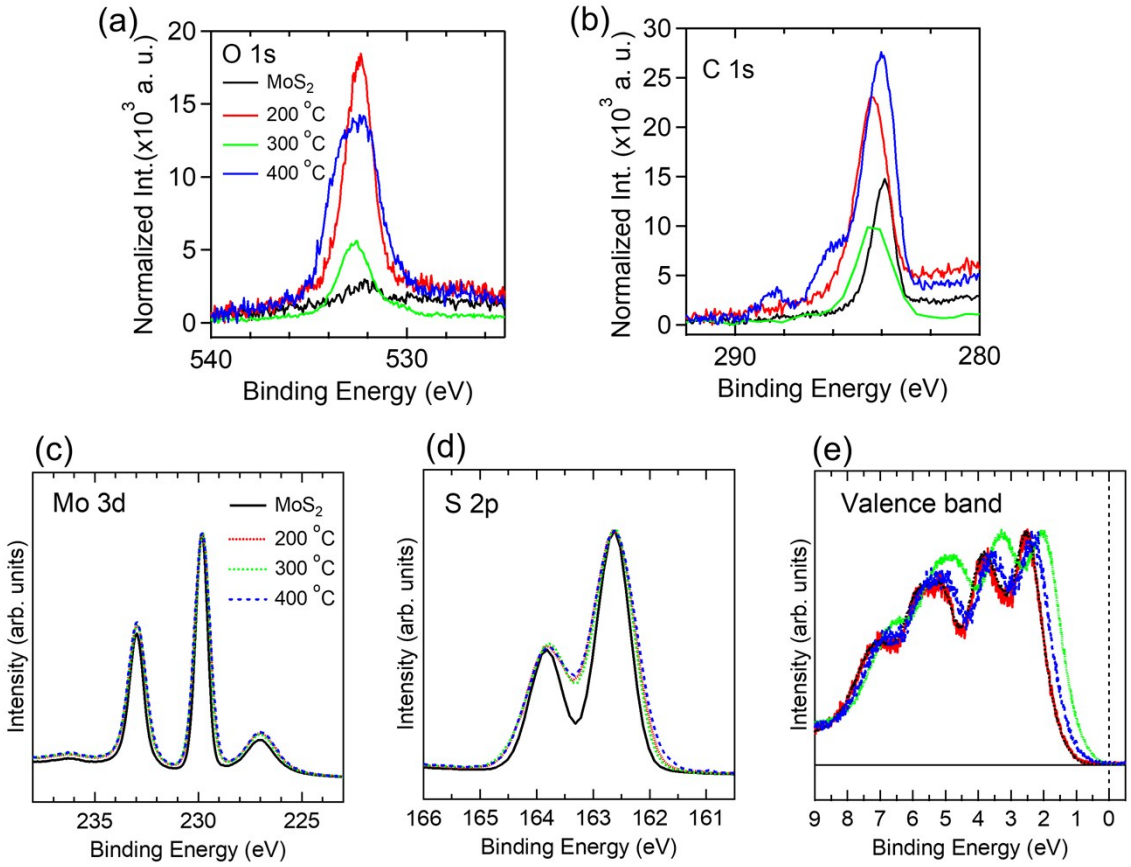

Boltzmann's constant, and T is the absolute temperature.

Fig. S2 (a)–(e) Comparison of O 1s (a), C 1s (b), Mo 3d (c), S 2p (d) core levels, and valence band (e) spectra. (c–e) For comparison, all spectra are scaled to their maximum peak. Especially Mo 3d (c) and S 2p (d) core-level spectra are aligned to the binding energies of pristine MoS_2.

XPS spectra were acquired using a Thermo Scientific K-Alpha spectrometer (Thermo Fisher) equipped with an Al-Kα X-ray source and an energy resolution of 0.5 eV under UHV conditions of 10^{-10} Torr. X-ray photoemission spectroscopy (XPS) measurements revealed that all sample surfaces were covered by carbon (C) and oxygen (O). The latter is rather inert to MoS_2, compared the former. When these are excluded (Table SI), the stoichiometry of the pristine and annealed MoS_2 samples retains the 1:2 ratio of MoS_2. From the curve-fitting results,[1] the natural (Lorentzian) line widths (LW, related to the core-hole lifetime) of Mo 3d (0.04 eV) and S 2p (0.08 eV) broaden 2.6 ~ 2.8-fold and 1.6 ~ 1.9-fold, respectively, after N_2 annealing. These suggest that Mo atoms are

more sensitive to impurities than S atoms. In addition, the broadened LWs are closely related to the changes in band widths and shapes of valence band spectra. The valence band maximum (VBM) of MoS_2 annealed at 300 ^oC is closer to the Fermi energy than the pristine MoS_2 by 0.5 eV, as shown in Figure S2e. This may be due to the reduction in optical bandgap as shown in Figure S1d–f. VBM has been shown to originate mainly from Mo *d* orbitals.[1] Therefore, N_2 annealing appears to generate S vacancies.

Table SI. XPS characterization results of the samples.

	Mo 3d (%)	S 2p (%)	O 1s (%)	C 1s (%)	Stoichiometry
MoS_2	27	55	1	17	$MoS_{2.08}$
200 ^oC	24	50	6	21	$MoS_{2.12}$
300 ^oC	20	42	7	30	$MoS_{2.11}$
400 ^oC	22	47	6	25	$MoS_{2.11}$

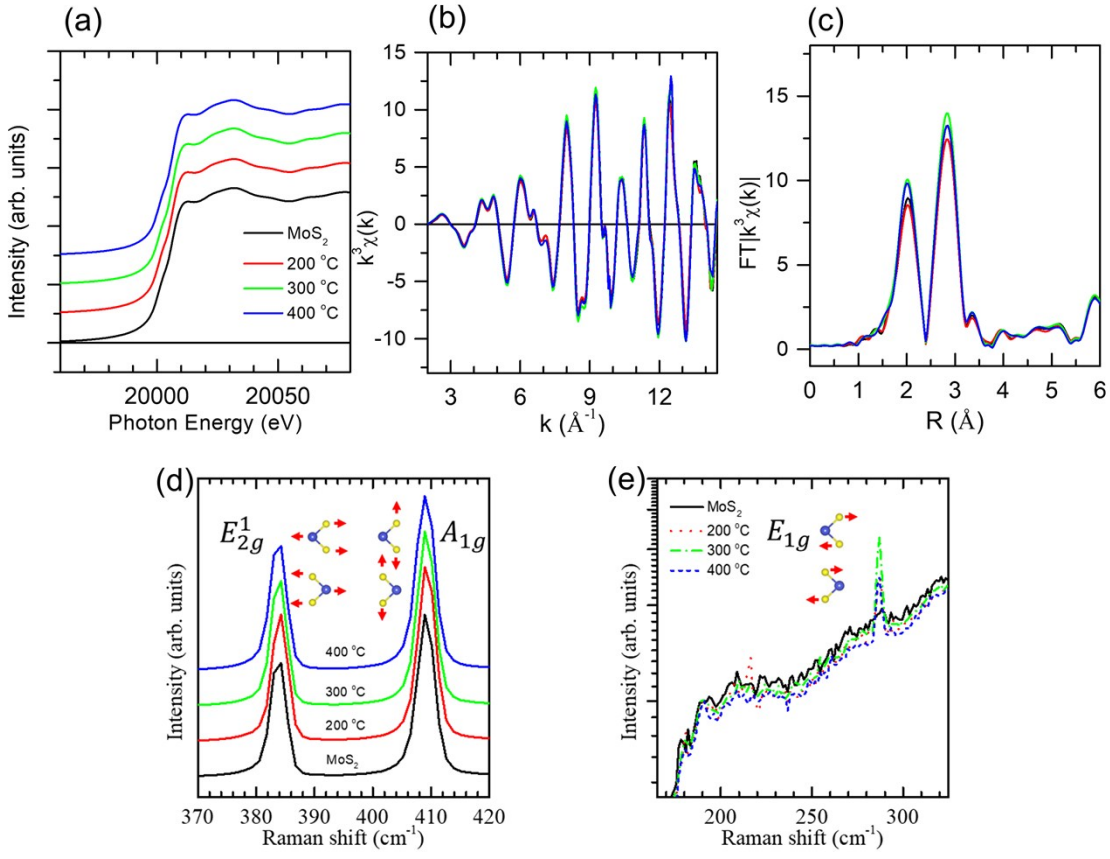

Fig. S3 (a)–(c) Mo K-edge x-ray absorption near edge structure, k^3-weighted EXAFS oscillations, and corresponding Fourier transforms. Two main peaks relate to Mo-S at 2.41 Å and Mo-Mo at 3.16 Å, respectively.

(d, e) Raman spectra with the corresponding E^1_{2g}, A_{1g}, and E_{1g} vibrational modes. Large blue and small yellow balls are Mo and S atoms. Different amplitudes are scaled to the A_{1g} mode.

EXAFS measurements were obtained at the 10C beamline of the PLS and EXAFS data were recorded in fluorescence mode at room temperature. The acquired data were processed and analysed using the program Athena and Artemis,[2] which implemented the FEFF6 and IFEFFIT codes.[3,4] The AUTOBK method[5] was used to isolate k-space EXAFS signals from the raw data, and a theoretical EXAFS signal was constructed using FEFF6. Raman spectra were obtained by a confocal Raman microscope using a Witec-Raman Confocal (Alpha 300R).

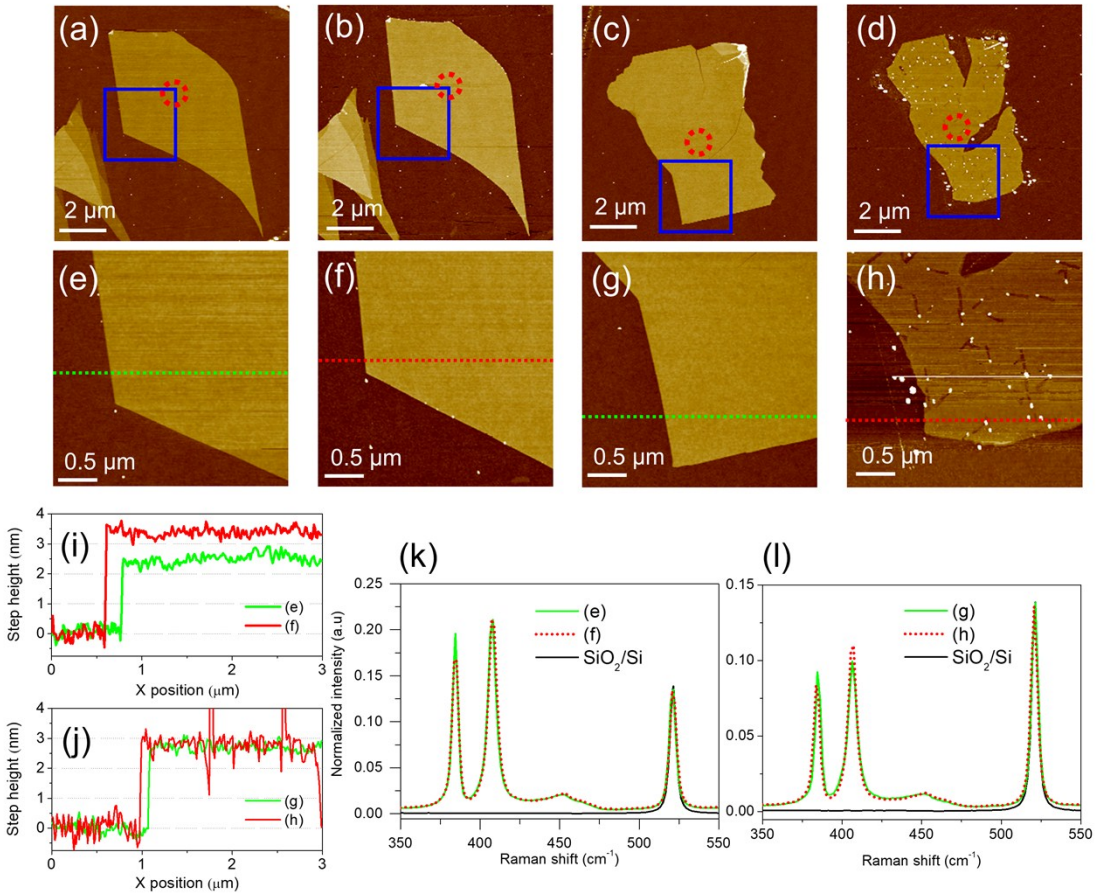

Fig. S4 (a)–(h) Atomic force microscopy (AFM) images. The mechanically exfoliated MoS_2 layers on the SiO_2/Si substrates (a, c) were annealed at 300 °C (b) and 400 °C (d) for 2hours in the furnace with filling the N_2 gas (N_2 annealing), respectively. The dotted circles (1 μm^2) in (a)-(d) indicate the positions for the Raman measurements.

(e)-(h) Magnified AFM images from the (blue square) insets of (a)-(d). (i)-(l) Comparison of the line profiles (i, j) of AFM images in (e)-(h) and the Raman spectra (k,l) before (e, g) and after (f, h) N_2 annealing.

Different to the bulk samples (Figure S3), the AFM and Raman result on the mechanically exfoliated few-layers of MoS_2 showed a delicate variation by N_2 annealing. The comparison of the AFM images between the initial (Figure S4a, S4e) and annealed few-layers of MoS_2 (Figure S4b, S4f) indicates that no significant change was obtained by N_2 annealing at 300 ^oC. However, as the temperature increased to 400 °C, the AFM images show that the cracked regions (Figure S4c) were severely etched (Figure S4d) with forming more cracks (Figure S4h). This result supports that the N_2 annealing at a higher temperature or longer time could result in the reduced interlayer distance of the annealed MoS_2 through the desulfurization (Figure 2d,e). The different, step height in Figure S4i is considered to be due to the chemical contrast of AFM noncontact mode. The small particles in Figure S4d and S4h are supposed to be the decomposed fragments of MoS_2.

On the other hand, Raman spectra (Figure S4k, S4l) show that the frequency difference between the E^1_{2g} and A_{1g} modes is of 23.5 and 21.7 cm^{-1} in Figure S4a and S4c, respectively. It means that the thicknesses for the former and latter correspond to the 3L (Figure S4a) and 2L (Figure S4c). After N_2 annealing the frequency difference was slightly increased. In detail, a least-square fit curve of Raman spectra using Lorentzian function reveals that the N_2 annealing at 300 and 400 ^oC induced the blue- and red-shifts of both E^1_{2g} and A_{1g} modes by 0.13 and 0.47 cm^{-1} and -087 and -0.13 cm^{-1}, respectively. The intensity ratio of A_{1g}/E^1_{2g} for the former and latter was increased from 1.75 to 1.80 and decreased from 1.91 to 1.81, respectively. These different changes by the different annealing temperature are supposed to relate to an in-plane uniaxial tensile (300 ^oC) and compressive (400 ^oC) strains, respectively.[6] Notably, the N_2 annealing at 400 ^oC increased the Lorentzian width of the E^1_{2g} peaks by 0.52 eV but decreased the A_{1g} peak by 1.03 eV. It could result from the lattice distortion caused by the decomposition.

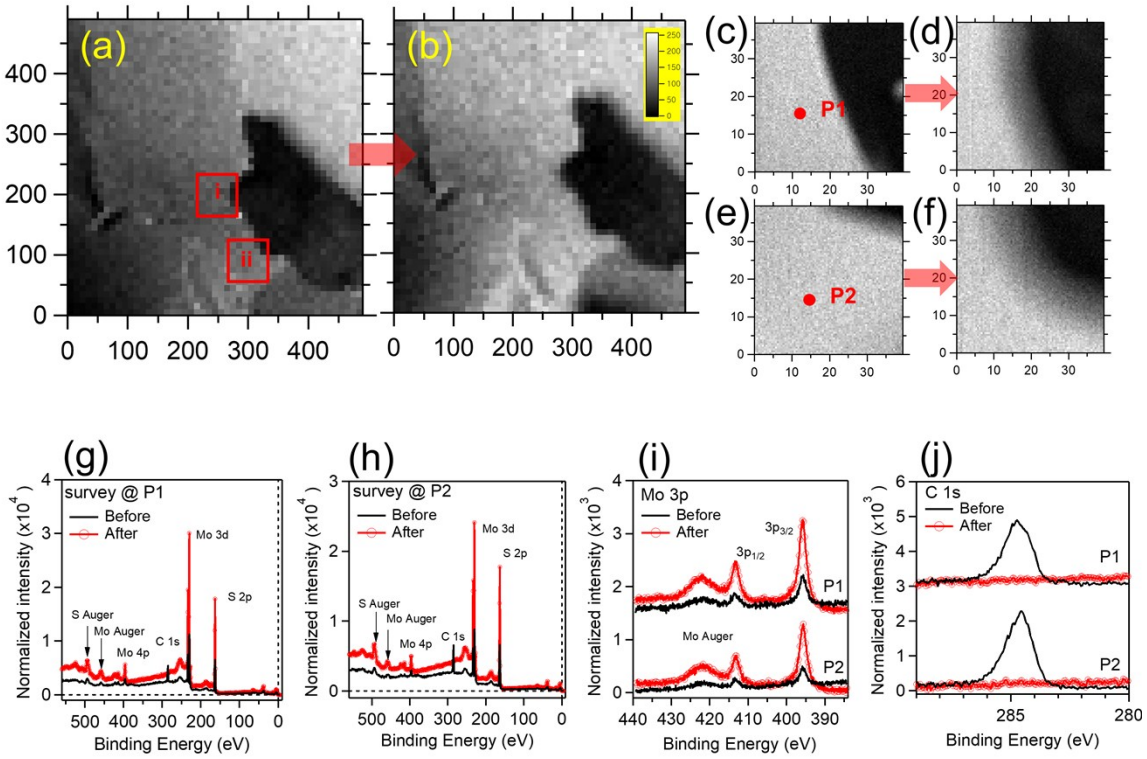

Fig. S5 (a–f) Comparison of SPEM images (μm^2) before (a), (c), (e) and after (b), (d), (f) UHV annealing of the *in-situ* cleaved MoS_2 surface. (c–f) Fine SPEM images were obtained at the positions of (i) and (ii) in (a). (g, h) Wide-scan, i, Mo 3p and N 1s, and j, C 1s core-level spectra were obtained at the spots labelled P1 and P2 in (c) and (e), respectively.

SPEM measurements were performed at the 8A1 beamline of the Pohang Light Source (PLS), Korea. For the SPEM measurement, single-crystalline bulk MoS_2 samples were cleaved in the UHV chamber (8×10^{-10} Torr) and then annealed at 300^{o}C for 2 h in nitrogen gas at a pressure of 1×10^{-6} Torr. SPEM images were taken using the selected energy channels of C 1s (280–290 eV), Mo 3d (226–238 eV), and S 2p (159–171 eV). The image obtained by the C 1s photoelectrons differed slightly compared to the others due to adsorbed carbon impurities on the cleaved MoS_2 surface even after cleavage in a UHV chamber. After taking the SPEM images, micro-spot photoemission spectra of the core levels and valence bands were obtained by focusing the beam on specific locations. The lateral resolution in SPEM mode was approximately 0.5 μm at a photon energy of 630 eV.

Notably, the O 1s core level disappeared after *in-situ* cleaving. Additionally, the N 1s core level is not observed in SPEM measurements (Figure S5i). These again confirm no interaction between the MoS_2 surface and N_2 gas. More remarkably, in contrast to the XPS results after N_2 annealing (Figure S2), the LWs of Mo 3d (0.04 or 0.06 eV) and S 2p (0.07 eV) core-level spectra were 1.5 ~ 2.5 and 1.2 ~ 1.3 times lower, respectively, after UHV annealing (Figure S6). These confirm that C adsorption on the MoS_2 surface results in broadening of MoS_2-related spectra for the N_2 annealed samples (Figure S2), and Mo atoms are especially sensitive.

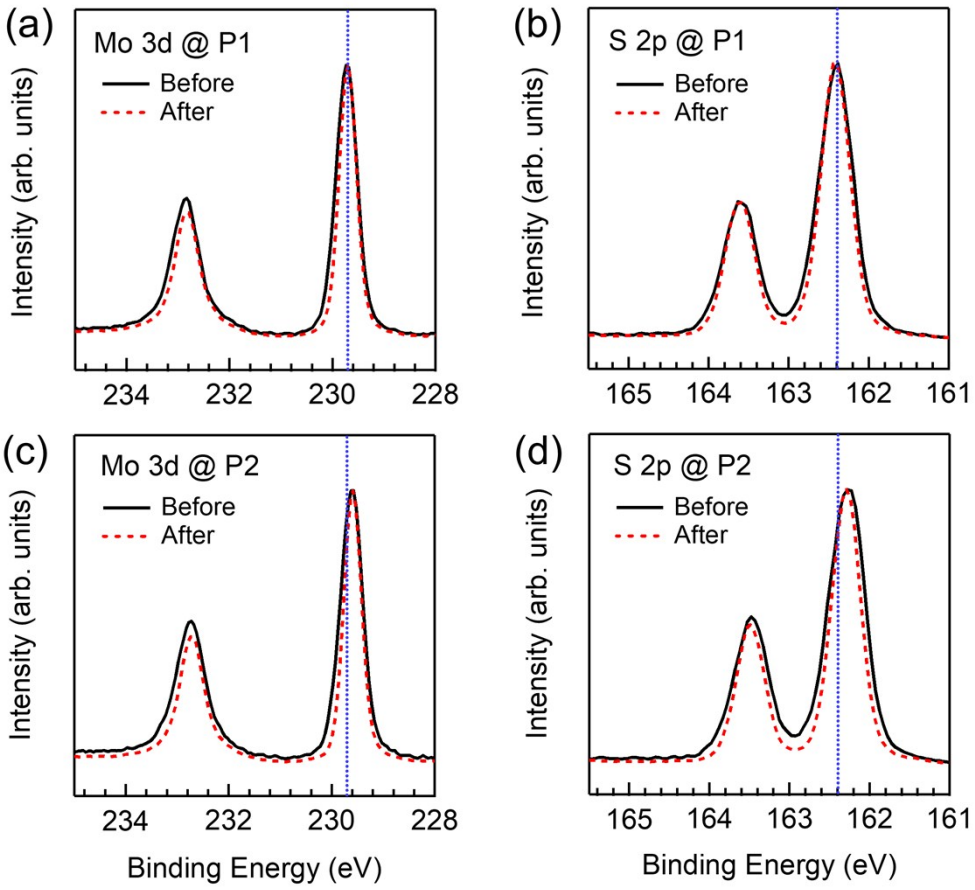

Fig. S6 (a–d) Comparison of the line shapes of Mo 3d and S 2p core-level spectra before and after UHV annealing.

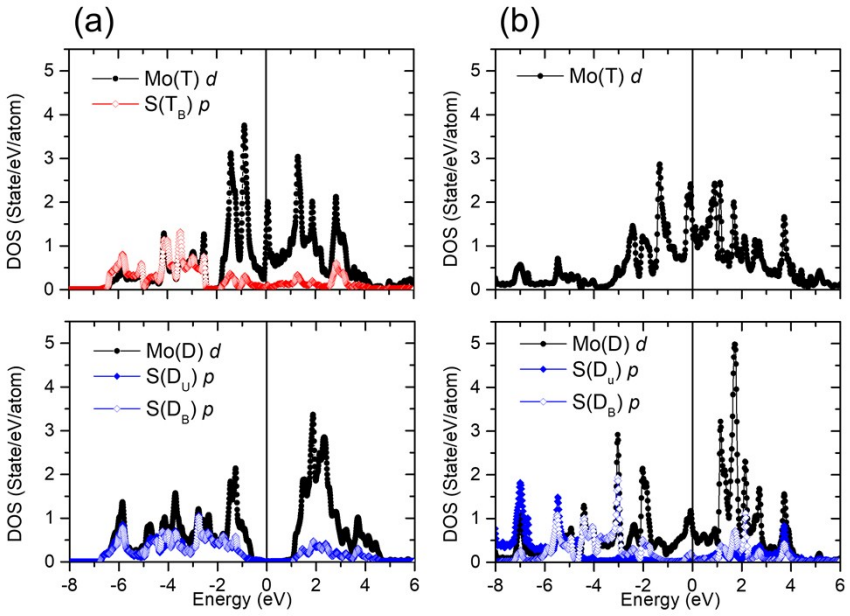

Fig. S7 (a, b) Density of states of corresponding configurations of Figure 4d and 4f. T, D, U, and B indicates top and down layers of MoS_2 bilayers with the corresponding upper and bottom S layers.

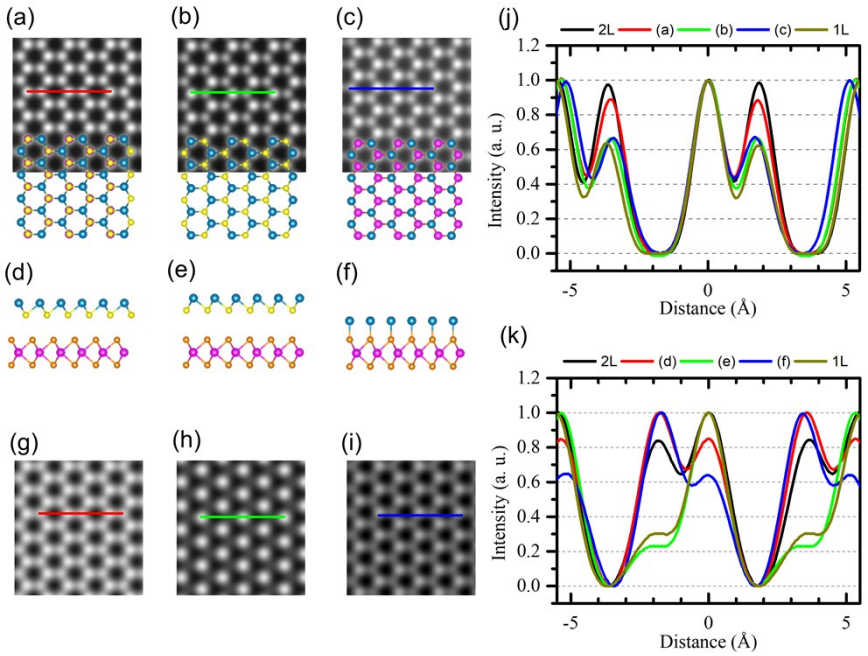

Fig. S8 (a–c) BF-STEM images (0-5 mrad) of corresponding configurations of Figure 4c, e, and f. (d-f), Top and side views of the corresponding atomic slabs of (a)-(c). (g–h) Corresponding HAADF-STEM images (150-200 mrad). (j, k) Intensity profiles of the selected lines in BF- (a–c) and HAADF (g–i) images with bilayer and monolayer (Figure 4) for comparison.

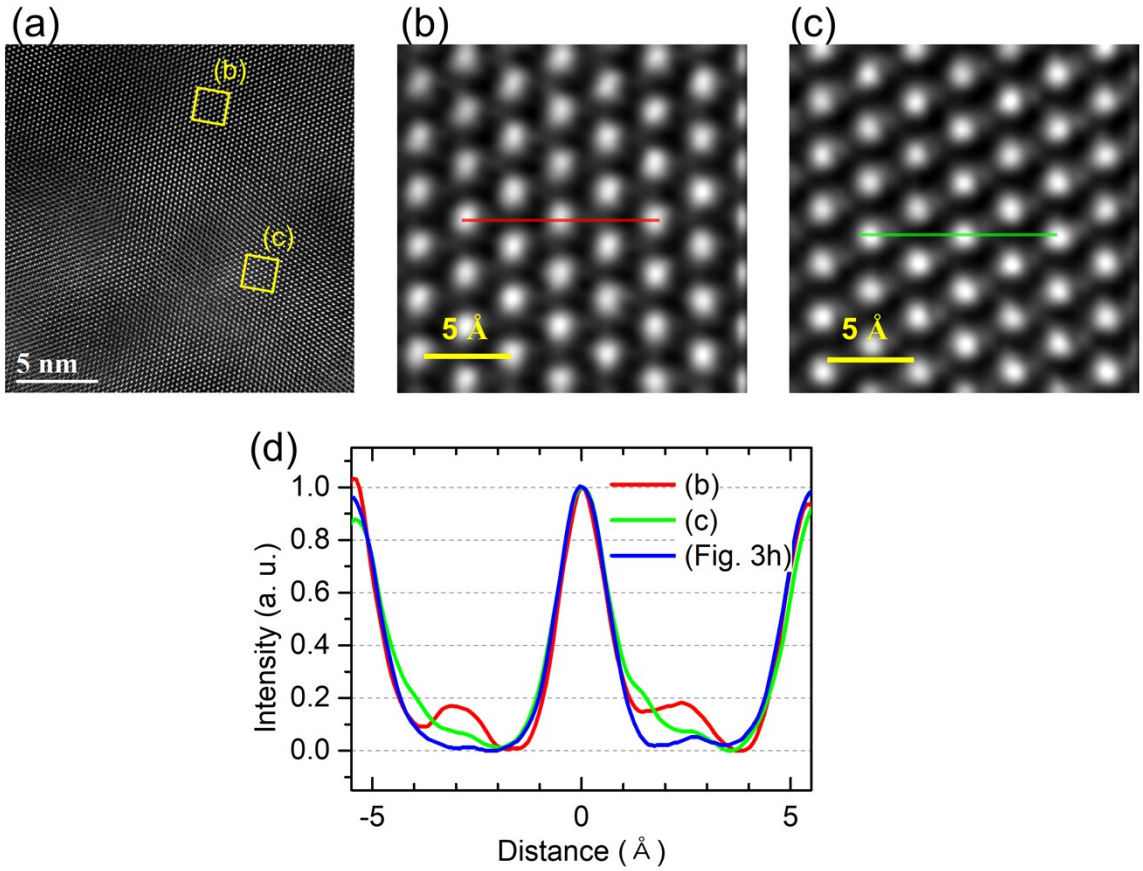

Fig. S9 (a) HRTEM image of Figure 3b. (b, c) Enlarged HRTEM images of the yellow-boxes in (a). (d) Intensity profiles of the selected lines in (b) and (c) with Figure 3h.

REFERENCES

1 S. W. Han, H. K. Kwon, S. K. Kim, S. Ryu, W. S. Yun, D. H. Kim, J. H. Hwang, J.-S. Kang, J. Baik, H. J. Shin and S. C. Hong. *Phys. Rev. B*. 2011, **84**, 045409.

2 B. Ravel and M. Newville, *J. Synchrotron Rad.* 2005, **12**, 537.

3 J. J. Rehr, R. C. Albers and S. I. Zabinsky, *Phys. Rev. Lett*. 1992, **69**, 3397.

4 M. Newville, *J. Synchrotron Rad.* 2001, **8**, 96.

5 M. Newville, P. Līviņš, Y. Yacoby, J. J. Rehr and E. A. Stern, *Phys. Rev. B.* 1993, **47**, 14126.

6 L. Yang, X. Cui, J. Zhang, K. Wang, M. Shen, S. Zeng, S. A. Dayeh, L. Feng, and B. Xiang, *Sci. Rep*. 2014, **4**, 5649.